Carbon Monoxide-Tolerant Platinum Nanoparticle Catalysts on Defect-Engineered Graphene

Gyubong Kim[†,‡] and Seung-Hoon Jhi[‡,§,*]

[†]Computational Science Center, Korea Institute of Science and Technology, Seoul 136-791, Republic of Korea, [‡]Department of Physics, and [§]Division of Advanced Materials Science, Pohang University of Science and Technology, Pohang 790-784, Republic of Korea

ABSTRACT We studied catalytic performance, particularly tolerance against CO poisoning and particle migration, of Pt nanoparticles dispersed on graphene using *ab initio* calculations. It was shown that the binding of Pt nanoparticles to graphene and the molecular adsorption on Pt can be controlled by introducing defects on graphene. Pt d-band center is a key parameter that is tailored by such defect formation. It is observed that the binding energy difference between H_2 and CO is well correlated with the d-band center, whereas individual H_2 and CO binding energies are not. Relative occupation ratio of H_2 on Pt in a CO environment showed that Pt nanoparticles can tolerate CO more than does bulk Pt when the particles are deposited on nitrogen-doped graphene.

KEYWORDS: platinum catalyst · fuel cell · graphene · nano clusters · *ab initio* calculation

Hydrogen oxidization is an important catalytic reaction in fuel cells. Pt catalysts are used at the anode of fuel cells where hydrogen oxidation reduction (HOR) occurs. Platinum (Pt) nanoparticles have received particular attention for their high catalytic efficiency and large surface area. Their size, shape, and substrate material affect their catalytic properties.[1−3] Comprehensive framework that can explain such variation of properties analytically is greatly desired. Pt particles are dispersed on various types of carbon materials (Pt/C), like carbon blacks. In such systems, the catalytic performance loss during extended operations is a critical problem due to the degradation of catalyst particles and the corrosion of the cathode support.[4] To overcome such drawbacks, carbon nanotubes (CNTs) have been proposed as a Pt support that may provide stronger Pt fixation than common carbon blacks.[4−6] But the interaction between Pt and such carbon materials and corresponding catalytic processes have not been systematically studied at atomic levels. Another important problem, particularly in proton-exchange membrane fuel cells (PEMFCs), is that even small fractions (>10 ppm) of CO can poison the anode, and this is one of the most serious obstacles to developing commercial fuel cell systems.[7−9] Solving these problems requires investigation of mechanisms at atomic or molecular levels. Pt nanostructures show versatile catalytic performance that depends on their size, shape, and support materials.[1−3] Factors that determine such reaction properties are complex, and many theoretical models have been proposed to characterize them using band profiles, orbital symmetries, and atomic bonding/relaxation conditions.[10−12] For nanoparticles, the complexity in morphology and in electronic and chemical properties complicates comprehensive analysis.

Here we investigate the degradation and CO contamination of Pt nanoparticles on graphene substrates. Like CNTs, graphene is a sp^2-bonded carbon material with a very large surface area and chemical stability for Pt support.[13,14] Each adsorption site on a Pt surface or cluster is occupied by one adsorbate species, and thus chemisorption of one CO molecule prohibits the adsorption of two H atoms.[9,15] Based on this observation, the thermodynamic feature of hydrogen reactivity can be quantified by the relative occupation ratio R, which is the ratio of adsorption sites occupied by hydrogen to those occupied by carbon monoxide:

$$R = \left(\sum^{N} [e^{(\mu_{H_2} - \varepsilon_{H_2})/kT}/(1 + e^{(\mu_{H_2} - \varepsilon_{H_2})/kT} + e^{(\mu_{CO} - \varepsilon_{CO})/kT})]\right)/N \quad (1)$$

where μ is the chemical potential and ε is the adsorption energy of each adsorbate, and the summation runs over the number of available adsorption sites N. In order to obtain the chemical potential μ as a function of pressure P and

*Address correspondence to jhish@postech.ac.kr.

Received for review July 22, 2010 and accepted December 20, 2010.

Published online January 04, 2011
10.1021/nn1017395

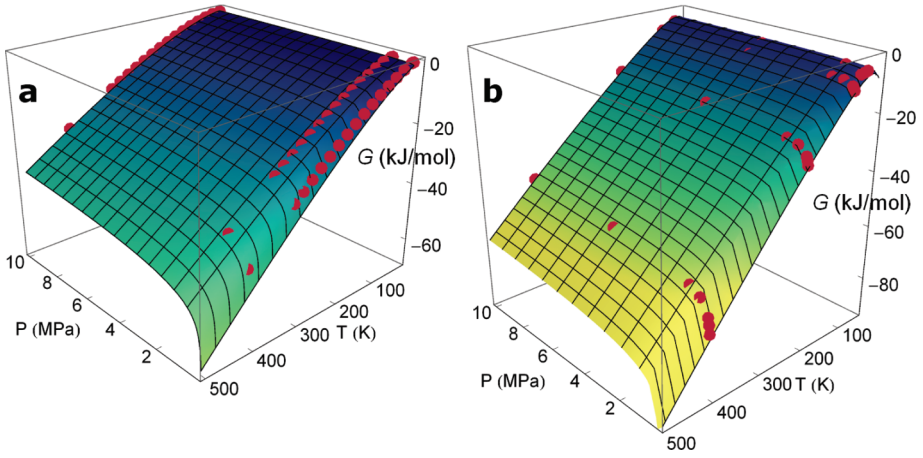

Figure 1. Gibbs free energy *G* (kJ/mol) of (a) H_2 and (b) CO fitted to experimental data (red dots) using eq 2. Note that *G* of CO shows a steeper variation in temperature than *G* of H_2.

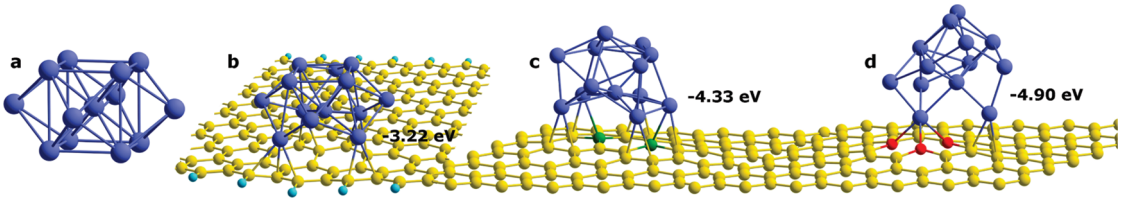

Figure 2. Optimized geometries of Pt_{13} (a) with (free-standing) D_{4h} symmetry and (b−d) adsorbed on graphenes: (b) on the zigzag (ZZ) edge of graphene nanoribbon (GNR); (c) on defective graphene with boron doping ($C_{96}B_2$); and (d) on defective graphene with nitrogen doping ($C_{94}N_3$). Blue balls: Pt atoms; yellow balls: carbon; green: boron; and red: nitrogen. The edge of GNR in (b) is passivated by hydrogen atoms (cyan balls). The binding energy (E_b) of Pt_{13} is given next to the clusters. Calculated E_b of Pt_{13} is −1.5 eV on the pristine graphene and −2.69 eV on the armchair (AC) edge, with an atomic configuration of Pt similar to (b). Due to the mismatch of bond length of Pt atoms to C−C distance, the morphology of Pt_{13} on (c) boron and (d) nitrogen defects differs from the highly symmetric shape in (a).

temperature *T*, we used the standard formula from the literature:[16]

$$G(P,T) = N_A\mu(P,T) = N_A[-aT\ln(T) + bT\ln(P) + c + dT + eT^2 + fT^3 + gT^4 + h/T] \quad (2)$$

where *G* is the Gibbs free energy, N_A is the Avogadro number, and a−h are the fitting parameters. Experimental data of the Gibbs free energies[17,18] were fitted using eq 2 (see Figure 1). *R* was then calculated as a function of *T* and partial pressure P_{CO} of CO. As *R* increases, Pt nanoparticles become more resistive to CO poisoning. In general, the adsorbate binding strength can change depending on the coverage. In our analysis, we made an approximation of using single molecular adsorption energy in calculating *R* by taking into account following two factors: First, in practice, CO partial pressure is much smaller than H_2 pressure, and its coverage will not be significant. The coverage of CO on Pt catalysts hardly exceeds 0.5 ML at ∼100 °C,[9] and CO tends to be well-dispersed even at such high coverage.[19] The intermolecular interaction and its effect on the adsorption energy can be neglected in this regime. Second, the hydrogen adsorption energies are quite insensitive to the change in coverage.[20,21] With these factors taken into account, our approximation is reasonable to study CO poisoning effect.

RESULTS AND DISCUSSION

Pt nanoparticles of ∼1 nm (∼several tens of atoms) in size have drawn interest as the best catalysts.[1,3] They have an adsorbate binding strength that is similar to that of a Pt bulk surface.[11,22] We chose Pt_{13} of D_{4h} symmetry, which is the most energetically favorable structure among the symmetrical isomers.[23] For comparison, we also considered Pt_6, a single Pt atom, and a Pt(111) surface (see Supporting Information). We introduced various forms of defects in graphene that can act as Pt binding centers and investigated the catalytic activity and corresponding adsorbate interactions of Pt. Most Pt atoms in Pt_{13} that bond to graphene sit at the carbon bridge sites except in pyridine-like N-doped graphene (PNG) (Figure 2). Due to mismatch of the bond length between Pt atoms and the carbon bridge, Pt clusters change their morphology on top of boron or pyridine-like nitrogen defects. The binding energy E_b of Pt_{13} on B or N defects is about three times larger than on pristine graphene (Figure 2). The strong binding of Pt to defective graphene prevents particle migration, which is a dominant process in degradation of Pt catalysts.

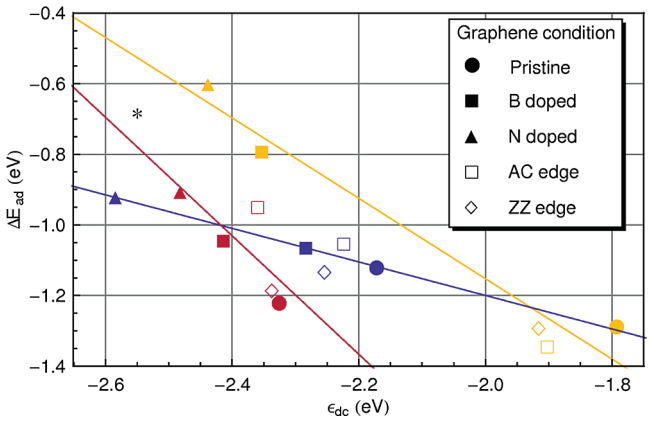

Figure 3. Averaged adsorption energy difference $\Delta E_{ad} = \bar{E}_{ad}(CO) - \bar{E}_{ad}(H_2)$ between H_2 and CO with respect to Pt d-band center (ε_{dc}) for Pt_1 (yellow), Pt_6 (blue), and Pt_{13} (red) deposited on defective graphene. Least-squares linear fits to data. Pt(111) surface case is also shown for comparison (black star). The fitted line for Pt_{13}, when extrapolated, is close to Pt surface data, indicating that Pt_{13} has similar catalytic characteristics as a Pt surface. Adsorption energies of individual molecules, $E_{ad}(CO)$ or $E_{ad}(H_2)$, on Pt_6 or Pt_{13} do not show any correlation with ε_{dc}, in contrast to the case of Pt atom or clean Pt surface. Small ΔE_{ad} implies a greater CO tolerance for H_2 adsorption (upper-left corner).

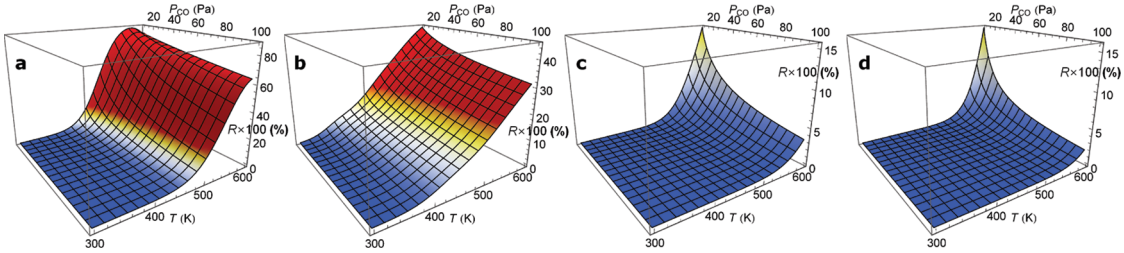

Figure 4. Relative occupation ratio R of hydrogen per adsorption site. (a) Pt(111); (b) Pt_{13} on PNG; (c) Pt_{13} on boron-doped graphene; and (d) Pt_{13} on armchair edges of GNR. Here hydrogen gas pressure = 0.1 MPa and R is calculated as a function of CO partial pressure P_{CO} and temperature T using chemical potentials obtained by fitting to experimental data (see Figure 1). Pt(111) surface shows excellent CO tolerance (large R) at high temperatures (>500 K) but a poorer tolerance at low temperatures. In contrast, Pt_{13} on PNG substrate has a better CO tolerance at low temperatures (300−500 K) than that of the Pt(111) surface. Other types of defects [see (c), (d), and Figure S2, Supporting Information] show very little improvement in CO tolerance even though $E_{ad}(H_2)$ is increased.

Experimentally, N-doped graphitic substrates were found to effectively disperse Pt nanoparticles and to improve the structural durability of Pt/C system; these results agree with our calculations.[24,25]

For clean Pt surfaces, the average energy ε_{dc} of d electrons (d-band center) of surface Pt atoms is highly correlated with the adsorbate binding strength.[26,27] However, for Pt nanoparticles or irregular surfaces that have complex morphology and electronic structure, such a simple model of correlation between ε_{dc} and molecular adsorption energies is not applicable in general.[10−12] In our calculations, the adsorption energy E_{ad} of hydrogen and CO on Pt nanoparticles does not show such a correlation, but the difference in averaged E_{ad} between H_2 and CO, $\Delta E_{ad} = \bar{E}_{ad}(CO) - \bar{E}_{ad}(H_2)$, was relatively well correlated to ε_{dc} of Pt clusters (Figure 3). Extrapolation of the plot of the correlation line for Pt_{13} suggests that Pt nanoparticles of such size would have molecular adsorption characteristics similar to that of a Pt(111) surface.[11,22] Because CO has stronger electron affinity than H_2, which indicates a larger amount of electron back donation from Pt, CO adsorption is more sensitive to the Pt d-band profile than is H_2 adsorption.[27] Figure 3 suggests that Pt nanoparticles would be the most tolerant to CO on PNG among tested graphene structures. Stronger binding of Pt to PNG lowers ε_{dc} and thus reduces ΔE_{ad}.

The difference in E_{ad} between CO and H_2 may hint at CO tolerance, but R in eq 1 gives clearer site-specific details. Calculated R explains the experimental observations of CO poisoning; at the PEMFC anode, 1% of CO blocks 98% of Pt active sites at ~300 K, and CO tolerance is considerably improved at temperatures >~400 K.[7−9] R for a Pt(111) surface (Figure 4a), a representative facet,[10,12] starts to increase at ~400 K in all CO concentration ranges consistent with such observation. The reduced Gibbs free energy of CO absorption has been suggested to be the origin of the greater CO tolerance of a Pt/C electrode at high temperatures.[7−9] However, calculated R clearly indicates that such CO tolerance is due to large negative μ_{CO} compared to μ_{H_2} at high temperatures (see Figure 1). Calculated R for Pt nanoparticles also shows greater CO tolerance at higher temperatures (>500K), but compared to a Pt(111)

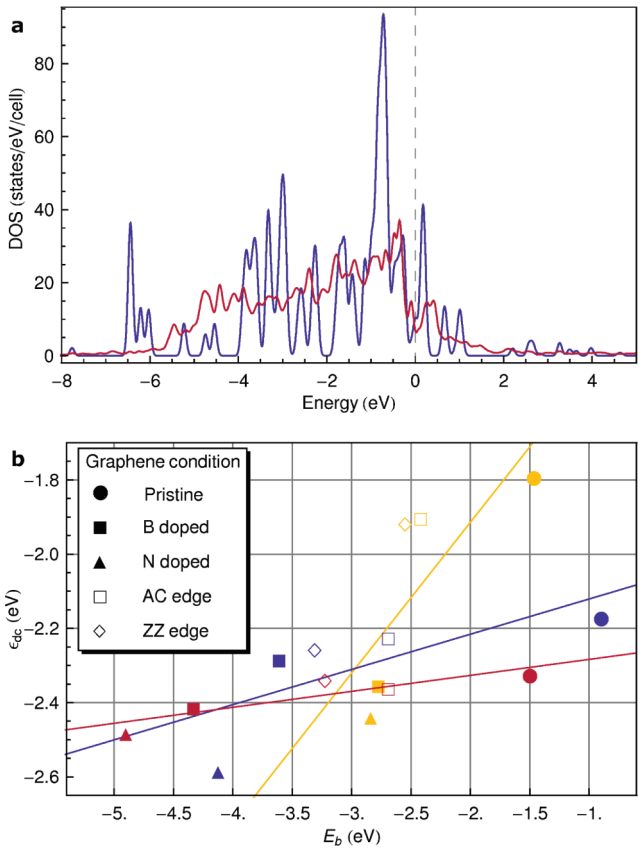

Figure 5. (a) Calculated density of states of free-standing Pt_{13} (blue) and Pt_{13} on PNG substrate (red). Dotted line: Fermi level set at zero energy. (b) Calculated d-band center (ε_{dc}) with respect to the binding energy (E_b) of Pt nanoparticles to defective graphene. Yellow, single Pt atom; blue, Pt_6; red, Pt_{13}; and lines: least-squares fits to the data. Positive correlation between E_b and ε_{dc} is noticeable.

surface, the CO tolerance of Pt nanoparticles is not better in this temperature range; this is because CO binds more strongly to them than to the Pt surface.[11] However, at practical PEMFC operating temperatures (300−500 K),[7,9] Pt_{13} nanoparticles deposited on PNG exhibit better CO tolerance than the Pt(111) surface (Figure 4a and b).

The relative occupation ratio R in eq 1 is a thermodynamic quantity and thus does not include the temporal behavior. Even with this limitation, our calculated values of R can be utilized to predict the characteristic poisoning time and to estimate the critical CO concentration for complete poisoning of Pt catalysts if we take the dynamic nature of R. In general, the kinetics of CO poisoning are determined by temperature, reaction area, gas pressure, and the energy barrier upon adsorption.[28] When the time dependence of $R = R(t)$, *i.e.*, its transient behavior, is considered, the calculated R from eq 1 is interpreted as $R = R(t \rightarrow \infty)$. True performance of Pt catalysts will be determined mostly by electrochemically active sites, whereas our calculation of R in eq 1 is about the relative coverage of all available binding sites. As a model process, we set the characteristic poisoning time at which time-dependent relative coverage of CO ($R_{CO}(t)$) exceeds the ratio of electrochemically active sites relative to all available binding sites (R_{AS}). We note that Figure 4 shows the calculated relative coverage for H_2 (R_{H_2}). It is reasonable to assume that Pt nanoparticles or rough Pt surfaces have larger R_{AS} than flat Pt surfaces. Once $R_{CO}(t)$ exceeds R_{AS}, the performance of Pt catalysts will degrade dramatically. In this respect, shrinking the size of Pt particles so that they have a larger R_{AS} or increasing the R_{H_2} (or decreasing R_{CO}) by changing the metal d level through N-doping of substrates will be effective ways to increase the poisoning time. Previous Monte Carlo simulations have also reported that the molecular adsorption rate and the specific poisoning time are highly correlated with the reaction area of the catalysts.[29] As for CO critical concentration, it can be taken as the value of CO partial pressure P_{CO}, below which R_{CO} never exceeds R_{AS} at given temperatures. The CO critical concentration is thus determined by setting $R_{CO}(t \rightarrow \infty) \approx R_{AS}$. For example, when we assume that Pt nanoparticles (Pt_{13}) have R_{AS} of 95% (*i.e.*, 95% among all available binding sites are electrochemically active for fuel cell functions), we obtain the CO critical concentration of about 50 ppm at 350 K. It is about 2 ppm for Pt(111) surface at the temperature if we assume the same R_{AS}. It increases to about 500 and to 40 ppm for Pt_{13} and Pt(111) surface, respectively, at 400 K. While determining R_{AS} is not straightforward at this moment, the relative occupation

R from eq 1 can provide a guide to estimate the critical CO concentration and to analyze the factors that affect it.

The charge transfer between molecules and Pt is critical in molecular adsorption on Pt. The correlation of ε_{dc} of Pt nanoparticles with the relative adsorption strength of CO and H_2 (Figure 3) indicates that engineering Pt binding on graphene can be an effective way to design CO-tolerant Pt particle catalysts. Pt nanoclusters adsorbed on CNT exhibit electronic structures strongly modified by the strong coupling between Pt and CNT.[5] Here we also observed a similar feature in Pt_{13} adsorbed on graphene. For example, the partial density of states projected on Pt nanoparticles that bind to PNG shows a significant broadening compared to free-standing Pt particles, which indicates a strong hybridization of Pt and graphene (Figure 5a). Also, the coupling of Pt d and graphene π orbitals lowers ε_{dc}; thus one can expect that as the binding between Pt nanoparticles and graphene becomes stronger, the d-band profiles will become broader and lower (Figure 5b). Other defects, such as carbon vacancy, have binding energies of metal atoms that are similar to that of PNG,[30] and mechanically induced porous CNTs significantly improve the dispersion of Pt particles and the CO tolerance in HOR.[31]

CONCLUSIONS

In summary, we investigated Pt nanoparticles dispersed on defective graphene substrates and their CO tolerance in hydrogen oxidization reaction. It was shown that defects in graphene increase Pt binding strength (E_b) significantly and lower Pt d-band center (ε_{dc}). The binding energy difference between CO and H_2 exhibits a strong correlation with Pt d-band center. Thermodynamic analysis shows that nitrogen doping in graphene improves CO tolerance of Pt nanoparticles. The results suggest that strong binding of Pt nanoparticles on defective graphene leads to enhancing the stability and CO poisoning. By optimizing E_b and ε_{dc}, Pt nanoparticle-based catalysts can be designed to be more resistant to degradation and less sensitive to CO poisoning. This kind of analysis will also provide a theoretical guide in other problems of chemical reactions in Pt-based catalysis.

METHODS

All calculations were performed using the first-principles total energy method, as implemented in the Vienna *Ab-Initio* Simulation Package[32] and employing the projector augmented wave pseudopotentials.[33] The electron exchange−correlation was treated within the spin-polarized generalized gradient approximation (GGA) in the form of Perdew−Burke−Ernzerhof-type parametrization.[34] The cutoff energy for the planewave basis expansion was chosen to be 400 eV, and the atomic relaxation was continued until Helmann−Feynman forces acting on atoms were <0.02 eV/Å.

Graphene supercells with a size of 4×4, 5×5, and 7×7 were used for Pt_1, Pt_6, and Pt_{13}, respectively, and the unit cell of graphene nanoribbons (GNRs) was chosen to have Pt-particle separation similar to that of graphene (Figure 2 and Supporting Information). The distance between graphene layers is 20 Å. The Brillouin zone was sampled using Γ-centered $5 \times 5 \times 1$, $3 \times 3 \times 1$, and $1 \times 1 \times 1$ *k*-point mesh for 4×4, 5×5, and 7×7 graphene, respectively; similar *k*-point grids were used for GNRs. The electronic levels were convoluted using Gaussian broadening with a width of 0.05 eV to obtain the density of states.

For simulating a Pt(111) surface, a 2×2 unit cell of four atomic layers was used, with the bottom layer frozen to the bulk Pt−Pt distance (~2.82 Å, as determined by our GGA calculation). The Brillouin zone was sampled using Γ-centered $8 \times 8 \times 1$ *k*-point grid. Fermi level smearing was done using the Methfessel−Paxton scheme[35] with a broadening width of 0.2 eV.

Acknowledgment. This research was supported by the National Research Foundation of Korea funded by the Ministry of Education, Science, and Technology (MEST) (grant no. 2009-0087731 and WCU program no. R31-2008-000-10059-0). G.K. was also partially supported by the Converging Research Center Program through the MEST (grant no. 2010K000992). This work was also supported in part by Korea Institute of Science and Technology Information (grant no. KSC-2009-S01-0021).

Supporting Information Available: CO and H_2 adsorption energies on Pt clusters. Calculated CO-tolerance function for all Pt_x-graphene structures. This material is available free of charge *via* the Internet at http://pubs.acs.org

REFERENCES AND NOTES

1. Vajda, S.; Pellin, M. J.; Greeley, J. P.; Marshall, C. L.; Curtiss, L. A.; Ballentine, G. A.; Elam, J.; Catillon-Mucherie, S.; Redfern, P. C.; Mehmood, F.; et al. Subnanometre Platinum Clusters as Highly Active and Selective Catalysts for the Oxidative Dehydrogenation of Propane. *Nat. Mater.* **2009,** *8*, 213–216.
2. Tsung, C.-K.; Kuhn, J. N.; Huang, W.; Aliaga, C.; Hung, L.-I.; Somorjai, G. A.; Yang, P. Sub-10 nm Platinum Nanocrystals with Size and Shape Control: Catalytic Study for Ethylene and Pyrrole Hydrogenation. *J. Am. Chem. Soc.* **2009,** *131*, 5816–5822.
3. Yamamoto, K.; Imaoka, T.; Chun, W.-J.; Enoki, O.; Katoh, H.; Takenaga, M.; Sonoi, A. Size-Specific Catalytic Activity of Platinum Clusters Enhances Oxygen Reduction Reactions. *Nat. Chem.* **2009,** *1*, 397–402.
4. Yu, X.; Ye, S. Recent Advances in Activity and Durability Enhancement of Pt/C Catalytic Cathode in PEMFC Part II: Degradation Mechanism and Durability Enhancement of Carbon Supported Platinum Catalyst. *J. Power Sources* **2007,** *172*, 145–154.
5. Cuong, N. T.; Fujiwara, A.; Mitani, T.; Chi, D. H. Effects of Carbon Supports on Pt Nano-Cluster Catalyst. *Comput. Mater. Sci.* **2008,** *44*, 163–166.
6. Tang, Z.; Poh, C. K.; Lee, K. K.; Tian, Z.; Chua, D. H. C.; Lin, J. Enhanced Catalytic Properties from Platinum Nanodots Covered Carbon Nanotubes for Proton-Exchange Membrane Fuel Cells. *J. Power Sources* **2010,** *195*, 155–159.
7. Baschuk, J. J.; Li, X. Carbon Monoxide Poisoning of Proton Exchange Membrane Fuel Cells. *Int. J. Energy Res.* **2001,** *25*, 695–713.
8. Cheng, X.; Shi, Z.; Glass, N.; Zhang, L.; Zhang, J.; Song, D.; Liu, Z.-S.; Wang, H.; Shen, J. A Review of PEM Hydrogen Fuel Cell Contamination: Impacts, Mechanisms, and Mitigation. *J. Power Sources* **2007,** *165*, 739–756.

9. Das, S. K.; Reis, A.; Berry, K. J. Experimental evaluation of CO poisoning on the performance of a high temperature proton exchange membrane fuel cell. *J. Power Sources* **2009,** *193*, 691–698.
10. Han, B. C.; Miranda, C. R.; Ceder, G. Effect of Particle Size and Surface Structure on Adsorption of O and OH on Platinum Nanoparticles: A First-Principles Study. *Phys. Rev. B: Condens. Matter Mater. Phys.* **2008,** *77*, 075410.
11. Xu, Y.; Getman, R. B.; Shelton, W. A.; Schneider, W. F. A First-Principles Investigation of the Effect of Pt Cluster Size on CO and NO Oxidation Intermediates and Energetics. *Phys. Chem. Chem. Phys.* **2008,** *10*, 6009–6018.
12. Wang, L.; Roudgar, A.; Eikerling, M. *Ab Initio* Study of Stability and Site-Specific Oxygen Adsorption Energies of Pt Nanoparticles. *J. Phys. Chem. C* **2009,** *113*, 17989–17996.
13. Seger, B.; Kamat, P. V. Electrocatalytically Active Graphene-Platinum Nanocomposites. Role of 2-D Carbon Support in PEM Fuel Cells. *J. Phys. Chem. C* **2009,** *113*, 7990–7995.
14. Pan, Y.; Gao, M.; Huang, L.; Liu, F.; Gao, H.-J. Directed Self-Assembly of Monodispersed Platinum Nanoclusters on Graphene Moiré Template. *Appl. Phys. Lett.* **2009,** *95*, 093106.
15. Chen, L.; Chen, B.; Zhou, C.; Wu, J.; Forrey, R. C.; Cheng, H. Influence of CO Poisoning on Hydrogen Chemisorption onto a Pt_6 Cluster. *J. Phys. Chem. C* **2008,** *112*, 3937–3942.
16. Johnston, K.; Castell, M. R.; Paxton, A. T.; Finnis, M. W. SrTiO3(001)(2 × 1) Reconstructions: First-principles Calculations of Surface Energy and Atomic Structure Compared with Scanning Tunneling Microscopy Images. *Phys. Rev. B: Condens. Matter Mater. Phys.* **2004,** *70*, 085415.
17. Lide, D. R.; Kehiaian, H. V. *CRC Handbook of Thermophysical and Thermochemical Data*; CRC Press: Boca Raton, FL, 1994.
18. Goodwin, R. D. Caron Monoxide Thermophysical Properties from 68 to 1000K at Pressures to 100 MPa. *J. Phys. Chem. Ref. Data* **1985,** *14*, 849–932.
19. Yeo, Y. Y.; Vattuone, L.; King, D. A. Calorimetric Heats for CO and Oxygen Adsorption and for the Catalytic CO Oxidation Reaction on Pt{111}. *J. Chem. Phys.* **1996,** *106*, 392–401.
20. Huda, M. N.; Kleinman, L. Hydrogen Adsorption and Dissociation on Small Platinum Clusters: An Electronic Structure Density Functional Study. *Phys. Rev. B: Condens. Matter Mater. Phys.* **2006,** *74*, 195407.
21. Wang, L.-L.; Johnson, D. D. Shear Instabilities in Metallic Nanoparticles:Hydrogen-Stabilized Structure of Pt_{37} on Carbon. *J. Am. Chem. Soc.* **2007,** *129*, 3658–3664.
22. Gruene, P.; Fielicke, A.; Meijer, G.; Rayner, D. M. The Adsorption of CO on Group 10 (Ni, Pd, Pt) Transition-Metal Clusters. *Phys. Chem. Chem. Phys.* **2008,** *10*, 6144–6149.
23. Aprá, E.; Fortunelli, A. Density-Functional Calculations on Platinum Nanoclusters: Pt_{13}, Pt_{38}, and Pt_{55}. *J. Phys. Chem. A* **2003,** *107*, 2934–2942.
24. Zhou, Y.; Pasquarelli, R.; Holme, T.; Berry, J.; Ginleyc, D.; O'Hayre, R. Improving PEM Fuel Cell Catalyst Activity and Durability Using Nitrogen-Doped Carbon Supports: Observations from Model Pt/HOPG Systems. *J. Mater. Chem.* **2009,** *19*, 7781–8016.
25. Zhou, Y.; Holme, T.; Berry, J.; Ohno, T. R.; Ginley, D.; O'Hayre, R. Dopant-Induced Electronic Structure Modification of HOPG Surfaces: Implications for High Activity Fuel Cell Catalysts. *J. Phys. Chem. C* **2010,** *114*, 506–515.
26. Nørskov, J. K.; Bligaard, T.; Rossmeisl, J.; Christensen, C. H. Towards the Computational Design of Solid Catalysts. *Nat. Chem.* **2009,** *1*, 37–46.
27. Pašti, I.; Mentus, S. DFT Study of Adsorption of Hydrogen and Carbon Monoxide on Pt_xBi_{1-x}/Pt(111) Bimetallic Overlayers: Correlation to Surface Electronic Properties. *Phys. Chem. Chem. Phys.* **2009,** *11*, 6225–6233.
28. Reuter, K.; Scheffler, M. First-principles Kinetic Monte Carlo Simulations for Heterogeneous Catalysis: Application to the CO Oxidation at RuO_2(110). *Phys. Rev. B: Condens. Matter Mater. Phys.* **2006,** *73*, 045433.
29. Albanoa, E. V.; Marro, J. Monte Carlo Study of the CO-Poisoning Dynamics in a Model for the Catalytic Oxidation of CO. *J. Chem. Phys.* **2000,** *113*, 10279–10283.
30. Kim, G.; Jhi, S.-H.; Lim, S.; Park, N. Effect of Vacancy Defects in Graphene on Metal Anchoring and Hydrogen Adsorption. *Appl. Phys. Lett.* **2009,** *94*, 173102.
31. Centi, G.; Gangeri, M.; Fiorello, M.; Perathoner, S.; Amadou, J.; Bégin, D.; Ledoux, M. J.; Pham-Huu, C.; Schuster, M. E.; Su, D. S.; et al. The Role of Mechanically Induced Defects in Carbon Nanotubes to Modify the Properties of Electrodes for PEM Fuel Cell. *Catal. Today* **2009,** *147*, 287–299.
32. Kresse, G.; Furthmüller, J. Efficient Iterative Schemes for *Ab Initio* Total-Energy Calculations Using a Plane-Wave Basis Set. *Phys. Rev. B: Condens. Matter Mater. Phys.* **1996,** *54*, 11169–11186.
33. Kresse, G.; Joubert, D. From Ultrasoft Pseudopotentials to the Projector Augmented-Wave Method. *Phys. Rev. B: Condens. Matter Mater. Phys.* **1999,** *59*, 1758–1775.
34. Perdew, J. P.; Burke, K.; Ernzerhof, M. Generalized Gradient Approximation Made Simple. *Phys. Rev. Lett.* **1996,** *77*, 3865–3868.
35. Methfessel, M.; Paxton, A. T. High-Precision Sampling for Brillouin-zone Integration in Metals. *Phys. Rev. B: Condens. Matter Mater. Phys.* **1989,** *40*, 3616–3621.